NIH Public Access
Author Manuscript
Acad Radiol. Author manuscript; available in PMC 2012 February 1.

Published in final edited form as:
Acad Radiol. 2011 February ; 18(2): 220–229. doi:10.1016/j.acra.2010.09.017.

A Preliminary Evaluation of Multi-Probe Resonance-Frequency Electrical Impedance based Measurements of the Breast

Bin Zheng, PhD, **Dror Lederman, PhD**, **Jules H. Sumkin, DO**, **Margarita L. Zuley, MD**, **Michelle Z. Gruss, BS, MTASCP**, **Linda S. Lovy, RT(R)(M)(CT), RDMS(BR)**, and **David Gur, ScD**
Department of Radiology, University of Pittsburgh, Pittsburgh, PA 15213, USA

Abstract

Rationale and Objectives—To preliminarily assess performance of a new, resonance-frequency-based electrical impedance signals (REIS) system in identifying young women who were recommended to undergo breast biopsy following imaging.

Materials and Methods—A seven probe REIS system was designed, assembled, and is currently being prospectively tested. During examination, contact is made with the nipple and six concentric points on the breast skin. Signal sweeps are performed and outputs ranging from 200 to 800 KHz at 5 KHz intervals are recorded. An initial set of 140 examinations including 56 that eventually had a biopsy, 63 who were negative during screening mammography, and 21 recalled for additional imaging but later determined as negative was used. An initial set of 35 features, 33 representing impedance signal differences between breasts and two representing participant age and average breast density, was assembled and reduced by a genetic algorithm to 14. Performance of an artificial neural network based classifier was assessed using a case-leave-one-out method.

Results—The substantially greater asymmetry between signals of mirror-matched regions ascertained from biopsy (“positive”) compared with non-biopsy (“negative”) cases, resulted in an ANN classifier performance (AUC) of 0.830±0.023. At 90% specificity this classifier, optimized for “recommendation for biopsy” rather than “cancer” detected 30 REIS “positive” cases (54%), including 6 of 9 (67%) actual cancers cases and 6 of 9 (67%) women recommended for surgical excision of high risk lesions.

Conclusions—Asymmetry in impedance measurements between bilateral breasts may provide valuable discriminatory information regarding the presence of highly suspicious imaging based findings.

Keywords

Electrical impedance spectroscopy (EIS); resonance frequency; risk stratification; breast cancer; artificial neural network; technology assessment

Correspondence: David Gur, University of Pittsburgh, Department of Radiology, Imaging Research, F.A.R.P. Building, 3362 Fifth Avenue, Pittsburgh, PA 15213-3180, Phone : 412-641-2513, Fax : 412-641-2582, gurd@upmc.edu.

Publisher's Disclaimer: This is a PDF file of an unedited manuscript that has been accepted for publication. As a service to our customers we are providing this early version of the manuscript. The manuscript will undergo copyediting, typesetting, and review of the resulting proof before it is published in its final citable form. Please note that during the production process errors may be discovered which could affect the content, and all legal disclaimers that apply to the journal pertain.

NIH-PA Author Manuscript
NIH-PA Author Manuscript
NIH-PA Author Manuscript

NIH-PA Author Manuscript

NIH-PA Author Manuscript

NIH-PA Author Manuscript

INTRODUCTION

Early detection of breast cancers in younger women (e.g. < 50 years old) is a mammographically difficult and time consuming task, primarily due to the low prevalence of disease and denser breast tissue (on average) that results in lower detection sensitivity and specificity [1–3]. In recent years, a number of alternative and/or improved approaches have been investigated for this purpose. Full-field digital mammography (FFDM), whole breast ultrasound (US), and magnetic resonance imaging (MRI) are frequently used for this purpose [4]. Other newer technologies such as digital breast tomosynthesis (DBT) and breast cone beam computed tomography (CBCT) are also being investigated [5,6]. These new breast imaging modalities have demonstrated the ability to achieve improved detection performance in specific groups of women as compared with film and/or digital mammography [7–9], resulting for example in the recent recommendation for periodic breast MRI examinations in women at high-risk as an adjunct to mammography [10]. Often these technologies result in the detection of different cancers; hence, the information obtained is complimentary to mammography [4]. However, all of these imaging modalities have well understood advantages and disadvantages, in particular when, and if, applied to a substantial fraction of the screened population with no known risk factors. Despite these advances and the fact that mortality from breast cancer is decreasing, there is a serious continuing controversy about the efficacy of current screening practices in the United States [11,12]. As related to women who are of pre-screening age and those not complying with screening recommendations at an older age, there has been an interest in developing an inexpensive, non-radiation based, simple to use and interpret examination tool that could be used during annual examinations at the physician's office in conjunction with the clinical breast examination (CBE). The underlying concept is that with the use of this new examination tool any abnormality in these women would be detected at an early time (and potentially at an earlier stage). Due to low cancer prevalence among younger women (e.g., < 50 years old), there may be an important role for tools that could stratify these women into two groups, the majority of those that are at "average risk" and but a small fraction of those (e.g., 10% or less) that are at significantly higher than average risk of having or developing breast cancer. Hence, women who do not participate in periodic imaging based screening because of their age, or their personal choice, and are found to be "positive" based on the stratification-type examination should be recommended to seek an imaging based evaluation because they were determined to belong to a "defined high risk group." [13]. This approach is then based on a "rule in" concept rather than a "rule out" one. Namely, such a stratification tool is in no way a competitor of imaging based surveillance. Under this paradigm, every additional cancer that would be ultimately detected as a result of the practice, and the imaging that would follow, will likely be detected substantially earlier. As important perhaps, a stratification-type examination (tool) with these operational characteristics could become extremely important for individualized screening recommendations if annual imaging based examinations, in particular at an earlier age (e.g., < 50 years old), is ultimately deemed to no longer be the standard of practice.

Electrical Impedance Spectroscopy (EIS) is one of the approaches that have been investigated for this purpose. Since the first imaging based EIS system to detect breast abnormalities was assembled and tested in the 1980s [14], a number of studies have followed [15–22]. The EIS approach involves the application of alternating low power electric signals into the testing sample (or target) followed by measurements of the sample's response. Differences in electrical conductivity and capacitance between neo-plastic and normal tissue have been shown in the 1920s and are thought to be primarily the result of changes in cellular water content, amount of extracellular fluid, blood flow, and membrane proteins [23]. It has long been established that cancer cells exhibit significantly different local dielectric properties as compared with normal cells [20]. For example, one study

NIH-PA Author Manuscript

NIH-PA Author Manuscript

NIH-PA Author Manuscript

reported that the conductivity and capacitance in malignant human breast tissue was 20 to 40 fold higher than in normal breast tissue [14]. A single breast imaging based commercial EIS system (T-Scan 2000, Mirabel Medical Systems, Austin, TX) was approved by the U.S. Food and Drug Administration as an adjunct modality to mammography [22]. The T-Scan 2000 uses a system-generated EIS signal mapping image of single breast contact and the EIS signal is inputted into a classifier designed for detection and classification of suspicious lesions. A number of studies of EIS signals acquired on breast tissue samples *in vitro* and breast surfaces *in vivo* demonstrated that measured EIS output signals contain some discriminatory information [24]. However, when applied to women in the clinic, the performance levels of EIS based classifiers remain relatively low. For example, the T-Scan 2000 has not been successful in terms of the stated objective as reported sensitivity was in the range of 20% to 30% at high specificity levels. Only one study reported 27% sensitivity at 94% specificity in a group of women that included 36 cancer and 476 negative cases [21].

We have been investigating a substantially different non-imaging based EIS concept in that the response signals we ascertain and analyze are specifically at and near the resonance frequency for the breast tissue being measured. We focus our analysis on asymmetry in measured EIS signals from mirror-matched regions of bilateral breasts of the examined woman [25–27]. Hence, we termed this approach resonance-frequency electrical impedance spectroscopy (REIS). The approach aims to identify younger women who are not routinely screened by an imaging modality but are at a higher than average risk of having or developing breast cancer. These women could then be recommended to undergo an imaging based follow-up. In a preliminary evaluation of a prototype REIS system with only one pair of probes, we demonstrated that there is relevant information in the measured signals and performance was statistically significantly better than chance [26]. Recently, we developed, assembled, and installed a new multi-probe REIS system [27]. Under an Institutional Review Board (IRB) approved protocol, we are currently conducting a prospective clinical data collection to assess the performance of this multi-probe REIS system. In this study, the initial set of REIS examinations acquired from 140 women with verified diagnostic results was used to develop and test an artificial neural network (ANN) based machine learning classifier. From the classification results of these women into “positive” (women actually recommended for biopsy) and “negative” (women not recommended for biopsy), we report here the preliminary assessment results.

MATERIALS AND METHODS

A. The multi-probe REIS system

Under an exclusive agreement between the University of Pittsburgh and Dhurjaty Electronics Consulting LLC (Rochester, NY), we designed and assembled a unique multi-probe REIS system (Fig. 1) that enables measuring and recording multi-channel output signal sweeps ranging from 200 to 800 KHz [27]. In brief, the system consists of a mechanical support, an electronic box with two sensor cups, and a notebook computer that includes the management software of the system control and data acquisition and recording. The two sensor cups have different surface curvatures specifically designed to fit “smaller” and “larger” breasts. Each sensor cup has seven mounted metallic probes. One probe is located at the center of the cup and the other six probes are mounted uniformly, or symmetrically distributed, along an “outer” circle with a 60mm radius. The probes (contacts) protrude approximately 4mm from the base of the cups to facilitate good contact with the breast. During an REIS examination, the center probe is intended to enable easy contact with the nipple. The other six external probes provide contact with six fixed points on the breast skin surface at a fixed distance to the nipple (center probe). Specifically, the six external probes are located at 12, 2, 4, 6, 8, and 10’o clock positions, respectively (Figure 1). The curvature of the cups and the distance between the probes were based on

NIH-PA Author Manuscript

NIH-PA Author Manuscript

NIH-PA Author Manuscript

actual multiple measurements using a mock-up device. The two sensor cups are mounted on the “front” and “back” of the electronic box. The complete assembly can be easily rotated 180° to allow use of either cup by the person conducting the REIS examination and is easily movable (up/down) to a desired height. The maximum electric voltage and current applied to the sensor probes are less than 1.5V and 30mA, respectively. Hence, applying a sensor cup to the breast skin is similar to physically holding a 1.5V battery between one’s fingers.

B. The REIS examination

After launching the REIS control software, a trained technologist performs the REIS examination as follows: 1) The technologist adjusts the height of the sensor box (lowers or raises) along a vertical rail (weight balanced for ease of use) to fit the height of the participant’s breast and locks it in place. The center probe is typically positioned slightly above the natural position of the participant’s nipple while standing. 2) The technologist selects the sensor cup to be used based on participant’s breast size and locks it in place. 3) The woman is asked to ‘lift” her breast slightly with her hand and position the nipple in contact with the center probe and then gently “pull herself into” the cup by holding one or both support sidebars designed specifically for this purpose. 4) The technologist keyboards a digital identification number specific to each REIS examination in a data entry window and then, using the computer mouse, initiates the REIS examination by clicking on a “start” command button displayed on the computer screen. Once the system detects (automatically done) that all seven probes are in “good contact with the breast”, signal acquisition commences. 5) The technologist visually monitors the signal scanning process on the computer screen to assure that contact between the breast skin and probes was maintained during the entire scanning period. If adequate contact is lost during the REIS examination, the system generates un-smoothed signal output curves and the examination results are discarded. A repeated examination is then conducted and recorded. A complete examination of each breast takes 8 seconds to scan, record, and save all measured output signals from as many as eight detection channels. During a complete REIS examination the same positioning and scanning protocol is performed on both breasts.

C. Acquired Output Signals

The recorded signal sweeps in each detection channel, namely a single pair of probes, includes three sets of output signals. Each records 121 output values for frequencies ranging from 200 KHz to 800 KHz at 5 KHz increments. The three sets of output signal sweeps represent signal amplitude (a), signal phase (p), and signal magnitude ($I = \sqrt{a^2 + p^2}$), respectively, as shown in Figure 2. At the resonance frequency, the signal magnitude (I) reaches a minimum output signal value and the phase signal crosses the $p = 0$ line (i.e. converts from a negative to a positive value). During each REIS examination, all generated and recorded six pairs of the three output signal sets are automatically saved in a computer database for future data analysis.

D. Study Participants

Under an IRB approved protocol we have been performing REIS examinations on consenting women between the ages of 30 and 50 years old who meet our inclusion criteria. Participants are classified based on actual diagnostic results (outcome) into one of three groups. The “positive” group includes women who had been recommended for biopsy following an imaging based diagnostic workup (BIRADS 4 or 5) and the REIS relevant examination was performed prior to the biopsy (typically on the same day approximately half an hour prior to the scheduled biopsy). The second group includes women who previously had a negative screening examination and were visiting our facility for their scheduled annual screening examination. Status verification in these women included at this

NIH-PA Author Manuscript

NIH-PA Author Manuscript

NIH-PA Author Manuscript

time, solely the negative mammograms of the scheduled screening examination. Currently we do not have long term follow-up on these women as it is scheduled to be performed in two years but the expectation value for future positive findings within one or two year is extremely low. The third group includes women who had been recalled for a diagnostic follow-up (BIRADS 0) as a result of a prior screening mammogram but were later (after a diagnostic workup) determined not to require a biopsy (BIRADS 1 or 2, no BIRADS 3 in this group). At this time our inclusion criteria for women who had been recalled for a diagnostic follow-up, or those who had been recommended for a biopsy, does not include restrictions regarding the type of abnormality in question (e.g. mass, cluster of micro-calcifications, focal asymmetry) or the specific location or depth of the suspected abnormality within the breast [26].

The multi-phase prospective clinical data collection task we are embarking on will be executed over the next two years and has several planned sequential analysis steps. As a preliminary assessment the first acquired set of 140 cases is reported here. We analyzed an initial set of 140 REIS examinations acquired with a new multi-probe based REIS system on women with known imaging and/or pathology based outcome. Among these women, 56 were “positive” (recommended for biopsy) and 84 were “negative” (non-biopsy) cases. The latter group (“negative”) included 63 that had not been recalled (screening negative) and 21 who had been recalled (screening BIRADS 0) for additional imaging procedures but were later determined not to need a biopsy (BIRADS 1 or 2); hence, these cases are considered “negative” for the purpose of this analysis. Among the 56 “positive” cases (BIRADS 4 or 5), imaging based examinations (i.e., mammography, ultrasound, and magnetic resonance imaging) showed that 37 cases depicted suspicious masses, asymmetric density, or architectural distortions, 8 depicted micro-calcification clusters alone, and 11 depicted both masses and micro-calcification clusters. Among the 56 biopsied lesions in this dataset, 16 were reported as “palpable” masses in the corresponding diagnostic reports (CBE), but only two of these eventually represented “high risk” lesions and none of the cancers were palpable. For the purpose of this analysis, the biopsy (“positive”) group included three types of cases, namely: (1) verified cancer cases, (2) cases with high risk lesions recommended for surgical excision, as a result of the biopsy that followed and (3) biopsy-proven benign cases. The biopsy results showed that the “positive” group included 9 cancer cases, 9 high risk cases and 38 benign cases. Among the 9 cancer cases, 4 depicted masses only, 2 were associated with micro-calcification clusters only, and 3 depicted both abnormalities. Among the 9 “high risk” cases, 6 depicted masses only, 2 depicted micro-calcification clusters only, and one depicted both abnormalities.

The average mass size in the biopsy group, as measured by ultrasound, was 1.37cm +/− 1.28cm (range 0.4cm to 7cm). The cancer mass sizes ranged from 0.85cm to 2.0cm. Among the 56 biopsied cases, 9 were located in the “peri-areolar” or “retro-areaolar” regions and 3 were located posterially, close to the chest wall. The remaining 44 biopsied lesions were reasonably well distributed in all breast regions. The average age of the women whose REIS data were included in this analysis was 43.8 ± 3.8 years old (with a range of 35 to 50 years old). Among the 140 cases in this dataset, 2 were subjectively rated by the radiologists during the imaging based examinations as being “almost all fatty” (1.4%), 32 were rated as “scattered fibroglandular densities” (22.9%), 93 were rated as “heterogeneously dense” (66.4%), and 13 were rated as “extremely dense” (9.3%).

E. The initial feature pool

A large number of EIS signal related features was extracted as the initial feature set from the six sets of EIS signal sweeps acquired between the center probe and each of the six “external” probes. We named each probe based on the location (orientation) of the external contact point at 12, 2, 4, 6, 8, and 10’o clock, respectively (Figure 1). Based on the

NIH-PA Author Manuscript

NIH-PA Author Manuscript

NIH-PA Author Manuscript

underlying assumption that, similar to asymmetry in tissue patterns, two breasts have a higher level of impedance symmetry in negative cases than in abnormal cases [20,25,26], we focused our analysis on signal differences between geometrically corresponding locations obtained from the two breasts of each participant. Figures 3 and 4 show typical signal sweeps (magnitude only) for a biopsy ("positive") case, and a non-biopsy ("negative") case, respectively.

The initial feature pool of 35 included 33 EIS signal based features and two non-EIS based features. The definitions of the initial 33 EIS signal based features follow. Feature 1 was defined as the maximum absolute difference between the ranges of all six resonance frequencies for each of the breasts as computed for the left (L) and right (R) breasts ($F_1 = Max\ |\Delta f_L - \Delta f_R|$). The remaining 32 EIS signal based features were divided into two distinct groups (Features 2 to 17 in group one and Features 18 to 33 in group two). In the first group, we averaged a number of EIS signal values of the six EIS sweeps (including both signal magnitude and phase) for each breast. Except for one feature that was computed as a mean of two averaged EIS signal values from the two breasts, the remaining 15 features were all computed by subtraction (differences) of two averaged EIS signal values from the two breasts. These 16 features were:

1. **Features 2 and 3:** We computed two average resonance frequencies including ($\bar{f}_L = (\sum_{i=1}^{6} f_i)/6$ for the left breast and $\bar{f}_R = (\sum_{i=1}^{6} f_i)/6$ for the right breast and defined the following two features. Feature 2 was the mean of the two averaged resonance frequencies ($F_2 = (\bar{f}_L + \bar{f}_R)/2$) and was the only feature that did not represent a subtracted value but rather represented the overall resonance frequency value as measured for the specific case. Feature 3 was the absolute difference between the two averaged resonance frequency values ($F_3 = |\bar{f}_L - \bar{f}_R|$).

2. **Feature 4:** By identifying the EIS signal magnitude value at the resonance frequency [$I(f)$] of each sweep and computing the average value of all six EIS sweeps ($\bar{I} = (\sum_{i=1}^{6} I(f)_i)/6$), we defined feature 4 as $F_4 = |\bar{I}_L - \bar{I}_R|$ representing the absolute difference in averaged EIS magnitude values at the respective resonance frequencies.

3. **Features 5 to 10:** Near each resonance frequency, we extracted six EIS signal magnitude values of an EIS sweep ($I(f_i)$) at six recorded frequencies, including two values smaller than the resonance frequency ($f_{-10} = f - 10$ KHz and $f_{-5} = f - 5$ KHz) and four values larger than the resonance frequency (from $f_5 = f + 5$KHz to $f_{20} = f + 20$ KHz at 5 KHz increments). For each of these extracted EIS magnitude values, we subtracted the EIS signal magnitude value at the resonance frequency of the same EIS sweep [$\Delta I_i = I(f_i) - I(f)$]. After computing the average EIS signal magnitude differences (ΔI_i) among all six probe pairs ($\Delta \bar{I}_i = \sum_{k=1}^{6} (\Delta I_i)_k$) for each breast, we defined six features ($F_j = |\Delta \bar{I}(f_i)_L - \Delta \bar{I}(f_i)_R|$, where $j = 5, 6, \ldots 10$, and $i = -10, -5, +5, +10, +15, +20$ representing the six frequency differences near the resonance frequency (in KHz) of the EIS signal sweeps). Thus, features 5–10 represented the absolute differences of the averaged EIS signal magnitude values between left and right breasts at these six frequencies.

4. **Feature 11:** Similar to the computation of feature 3 representing the difference in value between two frequencies, we computed another frequency difference value between two breasts based on the EIS signal phase sweeps (Figure 2). For each EIS

NIH-PA Author Manuscript

NIH-PA Author Manuscript

NIH-PA Author Manuscript

signal phase sweep, we identified the frequency at which the EIS phase value reaches a plateau [$f(p^{Max})$]. We then computed the average frequency value of the six EIS signal phase sweeps ($\overline{f}(p^{Max})=\sum_{i=1}^{6} f(p_i^{Max})/6$) for the left and the right breasts. We defined feature 11 as $F_{11}=|\overline{f}(p_L^{Max}) - \overline{f}(p_R^{Max})|$ representing the absolute difference between two averaged frequencies at which EIS phase values reach plateaus for the two breasts.

5. **Features 12 to 17:** Similar to features 5–10 we computed EIS signal phase value differences rather than EIS signal magnitude value differences for the same set of six frequencies of interest. Features 12 to 17 were defined as the absolute differences between two breasts of two averaged phase values at the specific frequencies, namely, $F_j = |\bar{p}(f_i)_L - \bar{p}(f_i)_R|$, where j = 12, 13, …17, and i = −10, −5, +5, +10, +15, +20KHz different to the resonance frequencies, respectively.

Features 18 to 33 in the second group were defined and computed in a similar manner to Features 2–17 in the first group with the exception that only one pair of mirror-matched EIS signal sweeps (rather than averages of all six sweeps) from the left and the right breasts were selected for computing these 16 features. Specifically, for each REIS examination (case), we compared the resonance frequency differences for the six sets of mirror-matched EIS pairs of sweeps. We then selected the one matched pair of EIS sweeps (e.g., at 10'o clock on right breast and 2'o clock on the left breast) that had the maximum resonance frequency difference among all six matched pairs of EIS sweeps. Table I summarizes the distribution of cases that had a maximum resonance frequency difference between the two breasts at each of the six mirror-matched pairs in the dataset used in this study. After selecting the examination specific matched pair we discarded all other (five) pairs and we repeated the same computation process that was used to define and compute features 2 to 17 (F_2 to F_{17}). This process resulted in a second group of 16 EIS signal and phase related features (F_{18} to F_{33}). Last, we added to the feature pool the participant's age (F_{34}) and the radiologist's subjectively rated density BIRADS during the mammographic interpretations (F_{35}). As breast density and age are well known to be correlated with risk, the rationale of adding the two non-REIS based input variables ("features") was to test whether, or not, our classifier optimization scheme is sensitive to inclusion or exclusion of these variables ("features").

F. Optimization and performance assessment of the machine learning classifier

Selection of an "optimal" feature set through the process of pruning redundant features is an important step in developing any data-driven computerized scheme designed for this purpose. In previous studies, we established a feature selection protocol using a genetic algorithm (GA) that has been tested and applied frequently to optimize different machine learning classifiers including Bayesian belief networks [28], the artificial neural networks (ANN) [29], and k-nearest neighbor algorithms based template-matching scheme [30]. In this study, we applied a similar GA-based feature selection protocol to reduce the feature pool and build an optimal ANN. The feed-forward ANN built in this study included three layers. The first (input) layer included N neurons that connect to N selected features, the second layer included M hidden neurons, and the third (decision) layer included one neuron that generates a likelihood score of a test case being "positive" for the endpoint of interest (or not). A publicly available GA software package [31] was modified and used with a specifically designed binary coding method and a GA fitness function [29] to select an optimal feature set and ANN structure. The ANN directly connects the detection scores to the input data of a receiver operating characteristic (ROC) fitting and analysis program that computes the area under the ROC curve (A_z value). To minimize over-fitting and maintain robustness of the ANN performance, a limited number of training iterations (1000), and a

NIH-PA Author Manuscript

NIH-PA Author Manuscript

NIH-PA Author Manuscript

large ratio between the momentum (0.9) and learning rate (0.01), was used. During the GA optimization step, the initial 100 chromosomes in the first generation were randomly generated by the scheme. After a specific GA chromosome was selected, a case-based leave-one-out method was used to assess the performance of the ANN-based classifier. The 140 classification scores generated by this process were inputted into a ROC fitting and analysis program (ROCKIT [32]) to compute the area under the ROC curve (A_z value). Thus, after each training cycle, the GA generated a performance score (A_z) for each chromosome. The GA chromosomes that produce higher A_z values have higher probabilities of being selected in generating new chromosomes using the method of crossover and mutation. The GA operation was terminated when it reached a global maximum performance level or a pre-determined number of growth generations/iterations (i.e., 100 in this study).

After the highest performing ANN based classifier was determined, we re-computed the performance level when classifying the 140 cases in our dataset into "positive" and "negative" groups. Using the case based leave-one-out testing method we recorded the final ANN-generated classification scores for each test case over the entire positive and negative set of cases. The performance level (e.g., area under the ROC curve) and its variability (95% confidence intervals) were analyzed. We note that the classifier was optimized for an "actionable" endpoint (i.e., recommendation to biopsy) rather than for cancer as an end point. This was done specifically for the purpose of the intended use of our proposed approach, rather than as a screening tool to identify cancer cases. Under this scenario we clearly underestimate the ability to identify cancer cases had the classifier optimized for actual cancer as an endpoint, but the results for "biopsy recommendations" are more generalizable in this scenario due to the number of cases in the different groups. However, under this suboptimal optimization we computed the changes in sensitivity levels for different types of cases (i.e., verified cancer cases, "high-risk" cases recommended for surgical excision of the lesions, and all other biopsy recommended but pathology proven as benign cases). We also evaluated the relationship between detection results and different breast based characteristics (including type of depicted abnormalities and breast tissue density ratings) at a predetermined set of specificity levels.

RESULTS

An example of the three recorded breast EIS output signal sweeps for one measurement channel (one pair of probes) is shown in figure 2. The six sets of EIS signal magnitude sweeps between the center probe and each of the six "external" probes are shown in figure 3 for a participant with a biopsy confirmed cancer and figure 4 for a participant determined by mammography to be negative. As previously discussed by other investigators [20] and shown in our own previous studies [25,26], these figures demonstrate that in general "negative" cases tend to exhibit a higher level of electrical impedance symmetry between the two breasts than "positive" cases.

After using a genetic algorithm for selecting an optimal feature set, we built and tested an ANN-based classifier that included 14 input features (neurons) and four hidden neurons. The 14 selected features included six from those representing differences in averaged EIS signal or phase (the first feature group), namely F_6, F_{10}, F_{11}, F_{12}, F_{13}, and F_{15}, and eight features selected from the differences of EIS signals in individual mirror-matched probe pairs (the second feature group), namely F_{19}, F_{20}, F_{21}, F_{25}, F_{26}, F_{28}, F_{29}, and F_{30}. The distribution of these 14 selected features also shows that two features represented frequency differences (F_{11} and F_{19}), six represented EIS signal magnitude differences (F_6, F_{10}, F_{20}, F_{21}, F_{25}, and F_{26}), and six represented EIS signal phase differences (F_{12}, F_{13}, F_{15}, F_{28}, F_{29}, and F_{30}). Interestingly, the two non-REIS signal based features, including age (F_{34}) and breast density (F_{35}), were not selected by the GA for inclusion in the optimized classifier, supporting the

NIH-PA Author Manuscript

NIH-PA Author Manuscript

NIH-PA Author Manuscript

general expectation that, unlike mammography, REIS examinations are largely independent of patient age and/or breast tissue density.

The overall performance of the ANN based classifier resulted in an area under the ROC curve (Figure 5) of $A_Z = 0.830$ with a 95% confidence interval for AUC [0.755, 0.890]. Table II shows performance levels of the ANN training and testing results as a function of the number of training iterations. Table III summarizes the detection results of the classifier, optimized for "biopsy" as an endpoint, at three predetermined specificity levels. The results are provided by biopsy outcome, type of abnormality, and density BIRADS. For example, the ANN classifier detected 30 "positive" (biopsy) cases or 54% sensitivity at 90% specificity.

DISCUSSION

As the number of women who participate in breast cancer screening programs increases, so too does the demand placed on the health care system to deliver high quality care to an ever increasing number of women through adequate access, high quality (accurate) interpretation, and at a reasonable cost. Despite the continuing controversy about the efficacy of screening, in particular as related to younger women, we believe that individualized risk based screening will ultimately be established and accepted in this country (and other countries as well for that matter). Despite the markedly lower prevalence of breast cancer at a younger age, there is great interest in improving early detection of breast abnormalities in younger women because of the large potential benefits. Identification of younger women who are at higher than average risk for having and/or developing breast cancer is an important and difficult task. This may even be more important in younger women who are not enrolled in annual mammography screening (e.g., < 40 years old in the US and < 50 years old in many other countries), or in women who choose for personal reasons not to participate in recommended imaging based screening programs. Among several alternative approaches to risk stratification that do not require radiation, electrical impedance based technology has been investigated extensively [13–21], but the results to date, using traditional EIS imaging based approaches, have been less than satisfactory [22].

Our focus on the development and assessment of a markedly modified EIS approach, namely a resonance-frequency based EIS approach (REIS) [25–27] that focuses primarily on signal asymmetry between bilateral breasts, may lead to an acceptable prescreening tool for this purpose. The unique characteristic of the REIS approach is that it does not only use information at the frequency range most likely to provide useful information, but it also weighs heavily on output signal differences between contra-lateral breasts of the same participant being examined. The multi-probe approach has a number of advantages. First, we are able to obtain a large amount of data points covering a reasonably large portion of the breast. Second, we can monitor in real time the quality of the physical contact between the different probes and the breast. Only when all seven probes have adequate contact the examination commences. Third, the data ascertainment period is short (8 seconds). To the best of our knowledge, no similar REIS system has been developed and/or is being tested for this purpose, to date.

When applied to this dataset, our multi-probe REIS system achieved a reasonably high performance level ($A_Z = 0.830 \pm 0.023$) as compared with our prior, rudimentary, single probe based REIS system ($A_Z = 0.707 \pm 0.033$) [26]. However, the two studies used different datasets acquired from different participants and therefore, one cannot directly compare the performance results of the two studies. For a more valid comparison we selected a single mirror-matched probe pair (at 10'o clock and 2'o clock for the left and right breasts) representing the geometrically nearest possible location to the previous prototype system.

NIH-PA Author Manuscript

NIH-PA Author Manuscript

NIH-PA Author Manuscript

The ANN based classifier using REIS signal features extracted solely from this pair of matched probes achieved a performance level of $A_Z = 0.689 \pm 0.035$ that is quite similar to the previously reported performance for the single-probe pair based system. Hence, as we focus on location specific, differences-based information for classification purposes, the multi-probe approach seems to be substantially better.

Although this is a preliminary study, we can make several observations regarding the results we obtained. First, despite a suboptimal optimization for classifying cancer from non-cancer cases, this classifier yielded better sensitivity levels in detecting cancer and high risk cases recommended for surgical excision than in detecting "biopsy recommended" cases that proved to be benign. For example, at 90% specificity, the classifier assigned/rated 67% (6/9) of the cancer cases and 67% (6/9) of the high-risk cases as "REIS positive", while only assigned 47% (18/38) of other biopsy-proven negative cases as "REIS positive." This trend was consistent at all specificity levels examined in this study (Table III). Second, the classifier is able to detect different types of breast abnormalities. For example, at 90% specificity, the classifier assigned/rated 30 biopsy cases as "REIS positive," which include 17 that depicted masses only, 6 that depicted calcifications only, and 7 that depicted both abnormalities representing 46%, 75%, and 64% of these three types of abnormalities, respectively. Third, the classifier assigned/rated "REIS positive" cases in all breast tissue density categories (BIRADS ratings). For example, among the 30 cases classified as "REIS positive" at 90% specificity, 5 were rated as BIRADS 2, 20 as BIRADS 3, and 5 as BIRADS 4 representing 42%, 56%, and 63% of the three breast density groups in the entire dataset. Fourth, the sensitivity of the classifier seems to not be dependent on lesion size or location, as two of the three (67%) lesions marked by radiologists as located posterially near the chest wall were correctly detected at 90% specificity. Although interesting, we caution against generalization of these results because of the limited data in different categories after sub-setting.

The REIS based approach does not require radiation exposure. At the same time, it is not an imaging based device. Identifying either the types or the locations of any breast abnormalities has not been attempted to date. Despite the limitations of this preliminary study, in particular in terms of sample size, our results suggest that REIS based technology could potentially be used as a prescreening tool aimed at identifying a case based risk of having or developing breast cancer. The ultimate goal of the approach that we are exploring is to provide a fast, low cost, easy to use, and non-radiation based prescreening tool that can be incorporated into physicians' practices for periodic examinations of women who do not participate in annual mammography based screening or those who are at a younger age (e.g. between 35 years old and commencement of periodic mammography screening). In this respect REIS can be seen as an adjunct or an alternative examination to the clinical breast examination (CBE). Any cancer identified under this scenario would not have been found until later and possibly at a greater stage during an eventual detection.

We note that REIS based examinations are not intended in any way to compete with imaging based screening mammography and it is not intended for screening women with known high risk factors. As related to imaging based screening, the REIS exam should be considered a "rule in" approach, namely given a positive REIS result the physician should consider recommending an imaging based follow-up examination, rather than using it as a "rule out" approach (i.e. women should not use a negative REIS result as an excuse to avoid imaging based screening).

At this stage our dataset is limited but we included both a relatively large set of "positive" cases (in this case women who after an imaging based diagnostic workup had findings that were suspicious enough to warrant a biopsy) and negative cases. The ratio of approximately

NIH-PA Author Manuscript

NIH-PA Author Manuscript

NIH-PA Author Manuscript

2:1 between negative and positive cases is higher than many preliminary optimizations of machine learning classifiers. Also, the testing procedures we implemented that included "recalled" but later determined to be "negative" cases, address at least in part the problem of generalization in terms of covering the "domain" from which the negative cases were selected. We note that in recruiting women to participate in this study, we did focus on recruiting pre-biopsy ("positive" for the purpose of this study) cases. This is a necessary, commonly implemented and generally accepted strategy in the medical imaging field for the purpose of developing and optimizing classifiers.

Despite the encouraging results showing that asymmetry in impedance signal measurements between the bilateral breasts may provide valuable discriminatory information regarding the presence of highly suspicious imaging based findings resulting in a recommendation for biopsy, we must emphasize that this is a preliminary study which suffers from a number of limitations. First, this study included a limited number of REIS examinations representing only a small subset of the examinations we plan to acquire in our ongoing prospective clinical data collection effort. Second, a direct comparison with results from other EIS based studies is not possible, as the participant pool is different and in this study we optimized the classifier for a surrogate endpoint, rather than cancer [15–22]. Third, all abnormalities included in this study had been originally detected on imaging based procedures, potentially biasing the results. We do not have data on performance when the REIS approach and classification scheme is applied to occult abnormalities during imaging. Last, whether or not the clinical use of this REIS approach would eventually result in a significant increase in unnecessary interventions due to false-positive findings has not been investigated in this preliminary study. Therefore, much work is needed in this area before we can conclude whether or not this approach should be prospectively tested for possible wide clinical use.

Acknowledgments

This work is supported in part by Grant 1R21/R33 CA127169 to the University of Pittsburgh from the National Cancer Institute, National Institutes of Health. The authors also thank the Magee-Womens Research Institute & Foundation, Glimmer of Hope Fund, for supporting this effort.

References

1. Smith RA. Breast cancer screening among women younger than age 50: a current assessment of the issues. CA Cancer J Clin 2000;50:312–336. [PubMed: 11075240]
2. Pisano ED, Gatsonis C, Hendrick E, et al. Diagnostic performance of digital versus film mammography for breast cancer screening. N Engl J Med 2005;353:1773–1783. [PubMed: 16169887]
3. Fenton JJ, Egger J, Carney PA, et al. Reality check: perceived versus actual performance of community mammographers. Am J Roentgenol 2006;187:42–46. [PubMed: 16794153]
4. Berg BA, Gutierrez L, NessAiver MS, et al. Diagnostic accuracy of mammography, clinical examination, US, and MR imaging in preoperative assessment of breast cancer. Radiology 2004;233:830–849. [PubMed: 15486214]
5. Poplack SP, Tosteson TD, Kogel CA, Nagy HM. Digital breast tomosynthesis: initial experience in 98 women with abnormal digital screening mammography. Am J Roentgenol 2007;189:616–623. [PubMed: 17715109]
6. Yang K, Kwan AL, Huang SY, et al. Noise power properties of a cone-beam CT system for breast cancer detection. Med Phys 2008;35:5317–5327. [PubMed: 19175091]
7. Warner E, Plewes DB, Hill KA, et al. Surveilance of BRCA1 and BRCA2 mutation carriers with magnetic resonance imaging, ultrasound, mammography, and clinical breast examination. Journal of American Medical Association 2004;292:1317–1325.

NIH-PA Author Manuscript

NIH-PA Author Manuscript

NIH-PA Author Manuscript

8. Kriege M, Brekelmans CT, Boetes C, et al. Efficacy of MRI and mammography for breast-cancer screening in women with a familial or genetic predisposition. N Engl J Med 2004;351:427–437. [PubMed: 15282350]
9. Gur D, Abrams GS, Chough DM, et al. Digital breast tomosynthesis: observer performance study. Am J Roentgenol 2009;193:586–591. [PubMed: 19620460]
10. Saslow D, Boetes C, Burke W, et al. American cancer society guidelines for breast screening with MRI as an adjunct to mammography. CA Cancer J Clin 2007;57:168–185. [PubMed: 17507442]
11. Berlin L, Hall FM. More mammography muddle: emotions, politics, science, costs and polarization. Radiology 2010;255:311–316. [PubMed: 20413746]
12. US Preventive Services Task Force, Screening for breast cancer: U.S. Preventive Services Task Force recommendation statement. Ann Intern Med 2009;151:716–726. [PubMed: 19920272]
13. Stojadinovic A, Nissan A, Shriver CD. Electrical impedance scanning as a new breast cancer risk stratification tool for young women. J Surg Oncol 2008;97:112–120. [PubMed: 18050282]
14. Chaundhary SS, Mishra RK, Swarup A, Thomas JM. Dielectric properties of breast carcinoma and surrounding tissues. IEEE Trans Biomed Eng 1988;35:257–263. [PubMed: 2834285]
15. Pipemo G, Frei G, Moshitzky M. Breast cancer screening by impedance measurement. Med Biol Eng 1990;2:111–117.
16. Malich A, Fritsch T, Anderson R, et al. Electrical impedance scanning for classifying suspicious breast lesions: first results. Eur Radiol 2000;10:1555–1561. [PubMed: 11044924]
17. Kerner TE, Paulsen KD, Hartov A, et al. Electrical impedance spectroscopy of the breast: clinical imaging results in 26 subjects. IEEE Trans Med Imaging 2002;21:638–645. [PubMed: 12166860]
18. Glickman YA, Filo O, Nachaliel U, et al. Novel EIS postprocessing algorithm for breast cancer diagnosis. IEEE Trans Med Imaging 2002;21:710–712. [PubMed: 12166870]
19. Sumkin JH, Stojadinovic A, Huerbin M, et al. Impedance measurements for early detection of breast cancer in younger women: A preliminary assessment. Proc SPIE 2003;5034:197–203.
20. Poplack SP, Paulsen KD, Hartov A, et al. Electromagnetic breast imaging: average tissue property values in women with negative clinical findings. Radiology 2004;231:571–580. [PubMed: 15128998]
21. Stojadinovic A, Nissan A, Gallimidi Z, et al. Electrical impedance scanning for the early detection of breast cancer in young women: preliminary results of a multicenter prospective clinical trial. J Clin Oncol 2005;23:2703–2715. [PubMed: 15837985]
22. Stojadinovic A, Moskovitz O, Gallimidi Z, et al. Prospective study of electrical impedance scanning for identifying young women at risk for breast cancer. Breast Cancer Res Treat 2006;97:179–189. [PubMed: 16491309]
23. Fricke H, Morse S. The electric capacity of tumors of the breast. J Cancer Res 1926;16:310–376.
24. Hope TA, Iles SE. Technology review: The use of electrical impedance scanning in the detection of breast cancer. Breast Cancer Res 2004;6:69–74. [PubMed: 14979909]
25. Sumkin JH, Zheng B, Gruss M, et al. Assembling a prototype resonance electrical impedance spectroscopy system for breast tissue signal detection: preliminary assessment. Proc SPIE 2008;6917:691–716.
26. Zheng B, Zuley ML, Sumkin JH, et al. Detection of breast abnormalities using a prototype resonance electrical impedance spectroscopy system: A preliminary study. Med Phys 2008;35:3041–3048. [PubMed: 18697526]
27. Gur D, Zheng B, Dhurjaty S, et al. Developing and testing a multi-probe resonance electrical impedance spectroscopy system for detecting breast abnormalities. Proc SPIE 2009;7263:72631F.
28. Zheng B, Chang YH, Wang XH, et al. Feature selection for computerized mass detection in digitized mammograms by using a genetic algorithm. Acad Radiol 1999;6:327–332. [PubMed: 10376062]
29. Zheng B, Chang YH, Good WF, Gur D. Performance gain in computer-assisted detection schemes by averaging scores generated from artificial neural networks with adaptive filtering. Med Phys 2001;28:2302–2308. [PubMed: 11764037]

NIH-PA Author Manuscript

NIH-PA Author Manuscript

NIH-PA Author Manuscript

30. Zheng B, Lu A, Hardesty LA, et al. A method to improve visual similarity of breast masses for an interactive computer-aided diagnosis environment. Med Phys 2006;33:111–117. [PubMed: 16485416]

31. Kantrowitz, M. Prime time freeware for AI, issue 1-1: selected materials from the Carnegie Mellon University, Artificial Intelligence Repository. Prime Time Freeware; Sunnyvale, CA: 1994.

32. Metz, CE. ROCKIT 0.9B Beta Version. University of Chicago; 1998. http://www-radiology.uchicago.edu/krl/

NIH-PA Author Manuscript
NIH-PA Author Manuscript
NIH-PA Author Manuscript

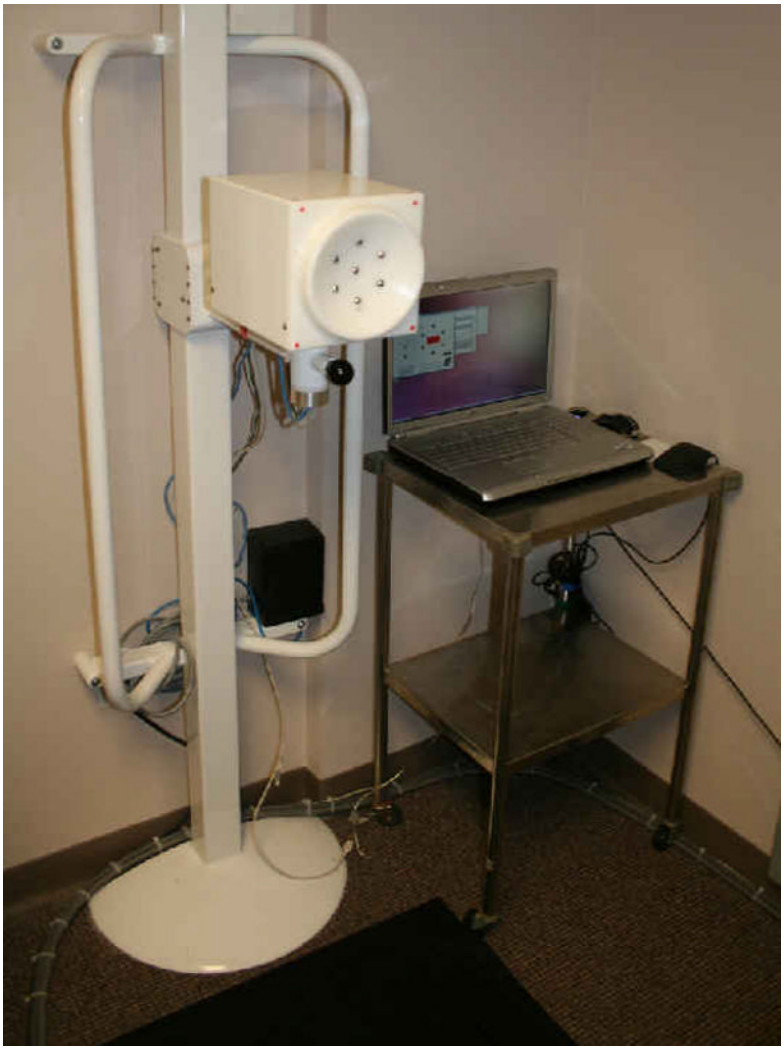

Figure 1.
The multi-probe REIS system installed in our clinical breast imaging facility.

NIH-PA Author Manuscript
NIH-PA Author Manuscript
NIH-PA Author Manuscript

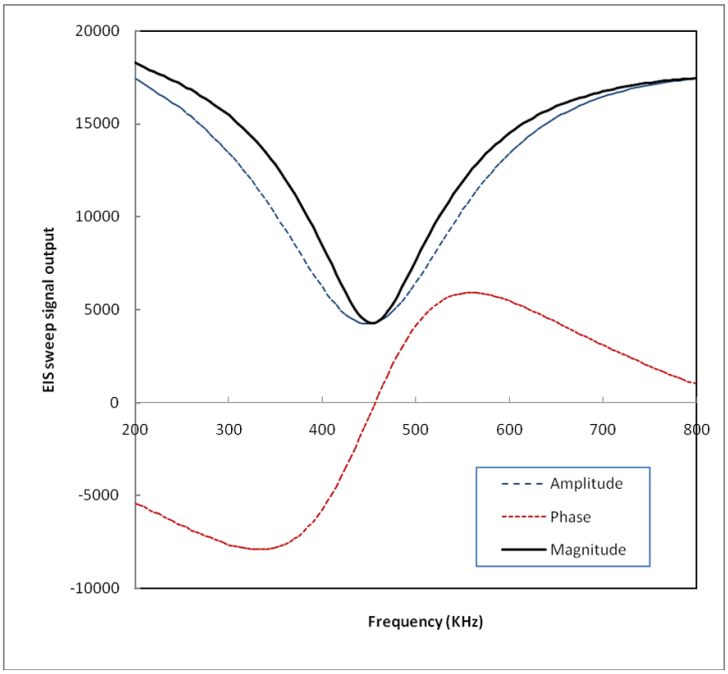

Figure 2.
An example of three recorded breast EIS output signal sweeps for a single probe channel.

NIH-PA Author Manuscript

NIH-PA Author Manuscript

NIH-PA Author Manuscript

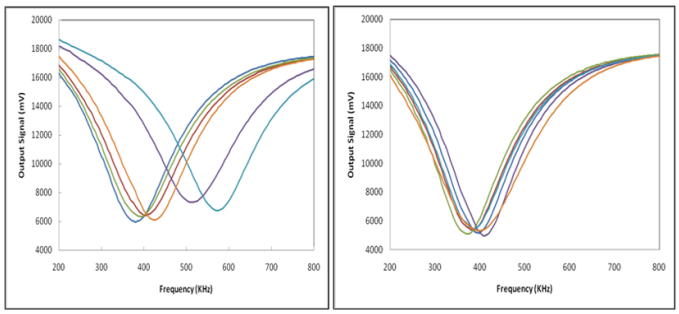

Figure 3.
Six sets of magnitude signal sweeps acquired from the right (a) and left (b) breasts of a 48 year old participant with a biopsy verified breast cancer.

NIH-PA Author Manuscript
NIH-PA Author Manuscript
NIH-PA Author Manuscript

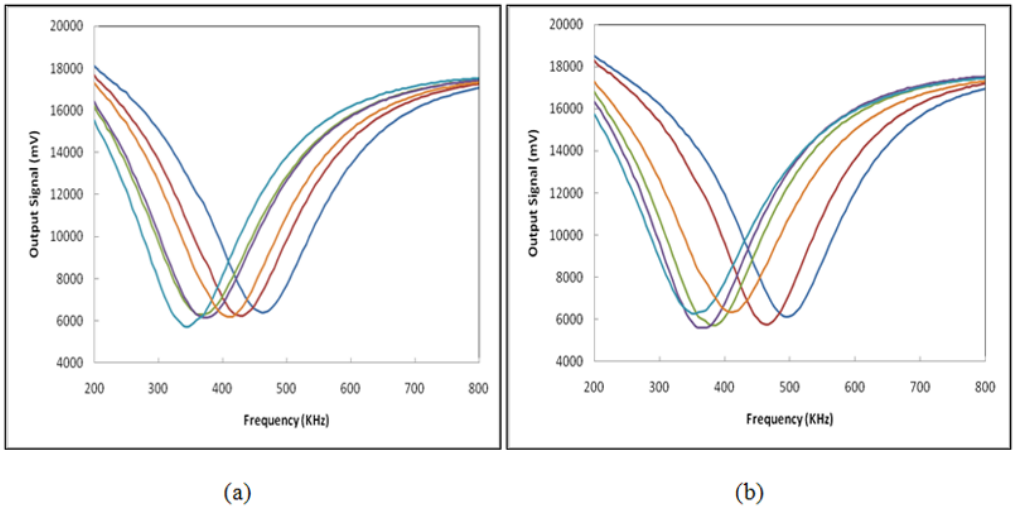

Figure 4.
Six sets of magnitude signal sweeps acquired from the right (a) and left (b) breasts of a 38 year old woman whose mammograms were rated “negative” during the screening mammography examination that followed the REIS examination.

NIH-PA Author Manuscript

NIH-PA Author Manuscript

NIH-PA Author Manuscript

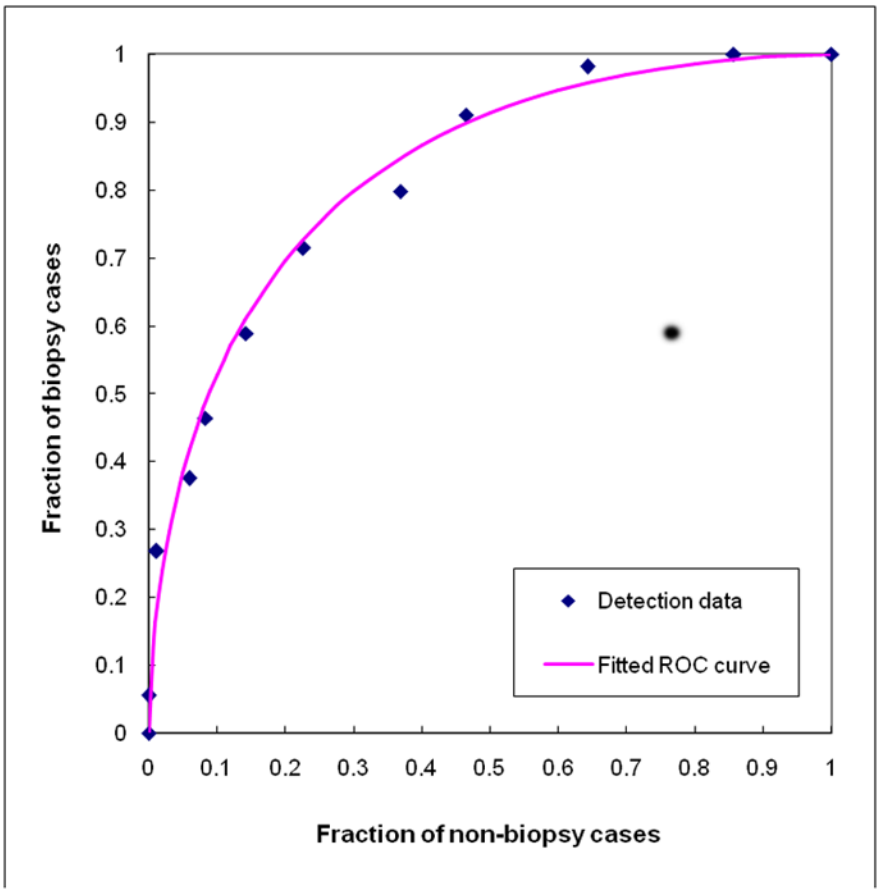

Figure 5.
Experimental ANN scoring (output) data and the fitted ROC curve for classifying 56 biopsy (positive) and 84 non-biopsy (negative) cases. The area under the ROC curve is 0.830 ± 0.023.

NIH-PA Author Manuscript
NIH-PA Author Manuscript
NIH-PA Author Manuscript

Table I

Number of occurrences by orientation (location) of the mirror-matched probe pair (out of six pairs) that showed maximum resonance frequency differences between two breasts.

Probe pair position on the left – right breast (o'clock)	12–12	2–10	4–8	6–6	8–4	10–2
Number of cases	34	27	18	19	10	32

NIH-PA Author Manuscript
NIH-PA Author Manuscript
NIH-PA Author Manuscript

Table II

The ANN overall classification performance levels measured by the areas under the ROC curves (A_Z values) and associated standard deviations as a function of the number of ANN training iterations.

Number of iterations	500	1000	1500	2000	3000
Training	0.873 ± 0.021	0.893 ± 0.017	0.901 ± 0.018	0.909 ± 0.018	0.922 ± 0.017
Testing	0.826 ± 0.025	0.830 ± 0.023	0.804 ± 0.026	0.783 ± 0.030	0.778 ± 0.031

NIH-PA Author Manuscript

NIH-PA Author Manuscript

NIH-PA Author Manuscript

Table III

Detection performance of the classifier by biopsy outcome, type of abnormality, and density BIRADS at three specificity levels.

	Specificity	95%	90%	80%
Biopsy result	All 56 biopsy cases	22 (39%)	30 (54%)	41 (73%)
	9 Cancer cases	2 (22%)	6 (67%)	7 (78%)
	9 High risk cases	6 (67%)	6 (67%)	7 (78%)
	38 Benign biopsy cases	14 (37%)	18 (47%)	27 (71%)
Abnormality	37 cases depicting only masses	14 (38%)	17 (46%)	25 (68%)
	8 cases depicting calcifications only	4 (50%)	6 (75%)	6 (75%)
	11 cases depicting both abnormalities	4 (36%)	7 (64%)	10 (91%)
Breast density	12 BIRADS 2 cases	3 (25%)	5 (42%)	9 (75%)
	36 BIRADS 3 cases	16 (44%)	20 (56%)	27 (75%)
	8 BIRADS 4 cases	3 (38%)	5 (63%)	5 (63%)